Dual Adaptive Dynamic Control of Mobile Robots using Neural Networks

Marvin K. Bugeja, *Graduate Student Member, IEEE,*
Simon G. Fabri, *Senior Member, IEEE,* and Liberato Camilleri

Abstract

This paper proposes two novel *dual adaptive* neural control schemes for the dynamic control of nonholonomic mobile robots. The two schemes are developed in discrete-time and the robot's nonlinear dynamic functions are assumed to be unknown. Gaussian radial basis function and sigmoidal multilayer perceptron neural networks are used for function approximation. In each scheme, the unknown network parameters are estimated stochastically in real-time, and no preliminary offline neural network training is used. In contrast to other adaptive techniques hitherto proposed in the literature on mobile robots, the dual control laws presented in this paper do not rely on the heuristic certainty equivalence property but account for the uncertainty in the estimates. This results in a major improvement in tracking performance, despite the plant uncertainty and unmodelled dynamics. Monte Carlo simulation and statistical hypothesis testing are used to illustrate the effectiveness of the two proposed stochastic controllers as applied to the trajectory tracking problem of a differentially driven wheeled mobile robot.

I. Introduction

The last two decades have witnessed an intense level of research activity on motion control of nonholonomic mobile robots [1]–[17]. This interest is primarily justified by a vast array of existing and potential practical applications [18]–[22]. In addition, a number of particularly interesting theoretical challenges enrich this field of study. In particular, most mobile robot configurations manifest restricted mobility, giving rise to nonholonomic constraints in their kinematics. Moreover, the majority of mobile robots are underactuated, having less control

Manuscript received Month XX, 200X; revised Month XX, 200X. This work was supported by National RTDI Grant 2004, RTDI-2004-026.

Marvin K. Bugeja and Simon G. Fabri are with the Department of Systems and Control Engineering, and Liberato Camilleri is with the Department of Statistics and Operations Research, University of Malta, Msida (MSD 2080), Malta.

inputs than degrees of freedom. Consequently, the linearized kinematic model of these robots lacks controllability; full-state feedback linearization is out of reach [3]; and pure smooth time-invariant feedback stabilization of the Cartesian model is unattainable [23].

Kinematic control, which dominated research efforts in the control of mobile robots for over a decade [1]–[3], [5], relies on the assumption that the control inputs, usually motor voltages, instantaneously establish the desired robot velocities. This outlook completely ignores the robot dynamics, and is commonly known as *perfect velocity tracking* [6]. In contrast, control schemes based on a full dynamic model [4], [6], [10], capture completely the behaviour of real mobile robots by accounting for dynamic effects due to mass, friction and inertia, which are otherwise neglected by kinematic control. However, the robot dynamic functions are nonlinear and include parameters that are often uncertain or even unknown, and which may also vary over time. These factors call for the development of nonlinear adaptive dynamic controllers to handle better unmodelled robot dynamics.

In response to these complex control issues, a number of advanced controllers have recently been proposed. Pre-trained function estimators, typically artificial neural networks (ANNs), have been used to render nonadaptive conventional controllers more robust in the face of uncertainty [12], [13]. These techniques require preliminary open-loop plant identification and remain blind to parametric and/or functional variations taking place after the training phase. Parametric adaptive control and robust sliding mode control, have also been proposed to mitigate the problem of unknown or uncertain mobile robot parameters [8], [10]. Another approach is that of online functional-adaptive control, where the uncertainty is not restricted to parametric terms, but covers the dynamic functions themselves [7], [11], [14]–[17]. We consider this approach to be more general and superior in handling higher degrees of uncertainty and unmodelled dynamics.

Adaptive controllers which have hitherto been proposed for the control of mobile robots, rely on the heuristic certainty equivalence (HCE) assumption [7], [11], [14]–[17]. This means that the estimated functions are used by the controller as if they were the true ones, thereby ignoring completely their uncertainty. When the uncertainty is large, for instance during startup or when the unknown functions are changing, HCE often leads to large tracking errors and excessive control actions, which can excite unmodelled dynamics or even lead to instability [24], [25].

In this paper we address these shortcomings via nonlinear stochastic adaptive control [24]. In stochastic adaptive control the uncertainty in the system is characterized by probability

distributions and their associated statistical measures. Moreover, an adaptive stochastic control law is a function of the parameter estimates as well as the uncertainty measures of these estimates. A major contribution in stochastic adaptive control is the *dual control* principle, introduced by Fel'dbaum [26]–[28]. A dual adaptive control law is designed with two aims in mind: (i) to ensure that the controlled output tracks the desired reference signal, with due consideration given to the estimates' uncertainty; (ii) to excite the plant sufficiently so as to accelerate estimation, thereby reducing quickly the uncertainty in future estimates. These two features are known as *caution* and *probing* respectively [25], [29]. Fel'dbaum showed that the exact solution of the *optimal* adaptive dual control problem can be derived using dynamic programming, specifically by solving the so called Bellman equation [26]–[28]. However, in almost all practical scenarios (with the exception of a few very simple cases [30]) this equation is impossible to solve, due to the very large dimensions of the underlying space [24], [25], [29], [31]. Consequently, a large number of *suboptimal* dual controllers have been proposed [25], [29], [31]–[35]. Although these suboptimal methods sacrifice optimality to render the algorithm computationally feasible, they are designed in a way to conserve the main dual features characterizing the optimal dual adaptive controller, namely *caution* and *probing*. In literature these suboptimal methods are further divided into two groups, namely *implicit* and *explicit* dual methods [25], [29]. The former type are based on various approximations of the optimal cost function [36], while the latter are based on a reformulation of the optimal adaptive control problem, so as the resulting solution is tractable but still maintains the much desired dual properties [25], [33], [37] possessed by the optimal controller. There are also a number of publications documenting successful practical applications of dual adaptive control [38]–[41].

The main contributions of the work presented in this paper are twofold. Firstly it is an extension of the control laws introduced by Fabri *et al.* [34] for the realization of dual adaptive control to intelligent neural network-based control systems. In this paper we propose two novel dual adaptive neural network controllers such that the work in [34] is generalized from the restricted single-input, single-output (SISO) case to the multiple-input, multiple-output (MIMO) nonlinear robot problem. The second main contribution is the investigation and statistical validation of the proposed dual control laws as applied to adaptive dynamic control of mobile robots. To the best of our knowledge, this application of dual control has not been previously investigated. We show that the proposed schemes lead to a significant improvement in performance as demonstrated by

extensive simulation results and a rigorous Monte Carlo statistical analysis.

Specifically, in this paper two novel dual adaptive neural control schemes are proposed for the dynamic control of nonholonomic mobile robots. ANNs are employed for the real-time approximation of the robot's nonlinear dynamic functions which are assumed to be unknown. The first scheme is based on Gaussian radial basis function (GaRBF) ANNs, and the second on sigmoidal multilayer perceptron (MLP) ANNs. The relative merits of each scheme are detailed later in the text. In each case, no preliminary offline neural network training is required, and the estimated functions and a measure of their uncertainty are *both* used in a suboptimal explicit dual adaptive discrete-time control law, which operates in cascade with a trajectory tracking kinematic controller. Each of the two schemes brings by a major improvement in tracking performance when compared to HCE control, under conditions of functional uncertainty and unmodelled dynamics.

Generally speaking the convergence and stability analysis of dual adaptive control schemes presents a very difficult challenge, mainly due to the stochastic and adaptive nature of the problem. The few works that address these issues consider only *linear* systems of a particular form and are characterized by a number of non-trivial assumptions [33], [42]. Consequently, to prove strict convergence and stability for a dual adaptive controller for a nonlinear system, is still considered to be an open problem within the research community. Hence in practice, as argued in [33], the stability of dual adaptive controllers is commonly checked by computer simulations and experimental applications. In this regard, we employ Monte Carlo simulation and statistical hypothesis testing to illustrate the effectiveness of the proposed control methods as applied to the trajectory tracking problem of a differentially driven wheeled mobile robot (WMR). Nevertheless, the employed framework is completely modular, and the presented dual adaptive dynamic controllers are valid also for different kinematic control laws that may be used to address other types of robot control problems such as posture stabilization and path following [3], [9].

The rest of the paper is organized as follows. Section II develops the stochastic discrete-time dynamic model of the robot. This is then used to design the dual adaptive controllers outlined in Section III. Monte Carlo simulations results and statistical hypothesis testing are presented in Section IV, which is followed by a conclusion in Section V.

II. MODELLING

This work considers the differentially driven WMR depicted in Fig. 1. The passive wheel is ignored and the following notation is adopted throughout the article:

P_o: midpoint between the two driving wheels

P_c: centre of mass of the platform without wheels

d: distance from P_o to P_c

b: distance from each wheel to P_o

r: radius of each wheel

m_c: mass of the platform without wheels

m_w: mass of each wheel

I_c: moment of inertia of the platform about P_c

I_w: moment of inertia of wheel about its axle

I_m: moment of inertia of wheel about its diameter

The robot state vector is given by $\boldsymbol{q} \triangleq [x \quad y \quad \phi \quad \theta_r \quad \theta_l]^T$, where (x, y) is the Cartesian coordinate of P_o, ϕ is the robot's orientation with reference to the xy frame, and θ_r, θ_l are the angular displacements of the right and left driving wheels respectively. The *pose* of the robot refers to the three-dimensional vector $\boldsymbol{p} \triangleq [x \quad y \quad \phi]$.

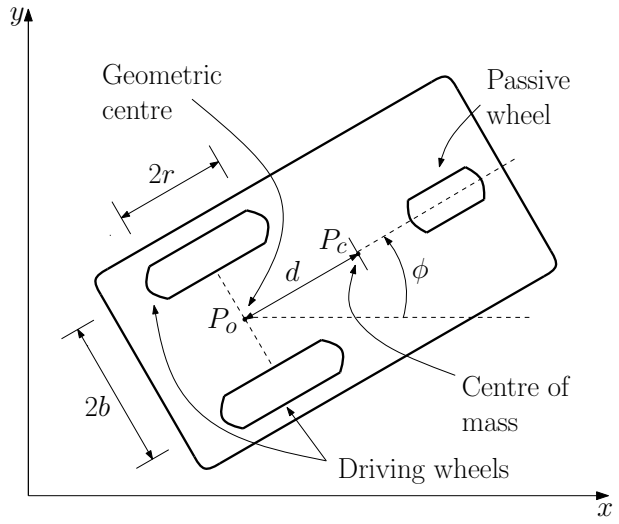

Fig. 1. Differentially driven wheeled mobile robot

A. Kinematics

Assuming that the wheels roll without slipping, the mobile platform is subject to three kinematic constraints (two of which are nonholonomic [4]), which can be written in the form $\boldsymbol{A}(\boldsymbol{q})\dot{\boldsymbol{q}} = \boldsymbol{0}$, where

$$\boldsymbol{A}(\boldsymbol{q}) = \begin{bmatrix} -\sin\phi & \cos\phi & 0 & 0 & 0 \\ \cos\phi & \sin\phi & b & -r & 0 \\ \cos\phi & \sin\phi & -b & 0 & -r \end{bmatrix}.$$

Furthermore, one can easily verify that $\boldsymbol{A}(\boldsymbol{q})\boldsymbol{S}(\boldsymbol{q}) = \boldsymbol{0}$, where

$$\boldsymbol{S} = \begin{bmatrix} \frac{r}{2}\cos\phi & \frac{r}{2}\cos\phi \\ \frac{r}{2}\sin\phi & \frac{r}{2}\sin\phi \\ \frac{r}{2b} & -\frac{r}{2b} \\ 1 & 0 \\ 0 & 1 \end{bmatrix}.$$

Hence, the kinematic model of this WMR is given by

$$\dot{\boldsymbol{q}} = \boldsymbol{S}(\boldsymbol{q})\boldsymbol{\nu}, \tag{1}$$

where $\boldsymbol{\nu}$ represents a column vector composed of the angular velocities of the two driving wheels, specifically $\boldsymbol{\nu} \triangleq [\nu_r \quad \nu_l]^T \triangleq \left[\dot{\theta}_r \quad \dot{\theta}_l\right]^T$.

B. Dynamics

The equations of motion of this WMR are given by the matrix equation

$$\boldsymbol{M}(\boldsymbol{q})\ddot{\boldsymbol{q}} + \boldsymbol{V}(\dot{\boldsymbol{q}}, \boldsymbol{q})\dot{\boldsymbol{q}} + \boldsymbol{F}(\dot{\boldsymbol{q}}) = \boldsymbol{E}(\boldsymbol{q})\boldsymbol{\tau} - \boldsymbol{A}^T(\boldsymbol{q})\boldsymbol{\lambda}, \tag{2}$$

where $\boldsymbol{M}(\boldsymbol{q})$ is the inertia matrix, $\boldsymbol{V}(\dot{\boldsymbol{q}}, \boldsymbol{q})$ is the centripetal and Coriolis matrix, $\boldsymbol{F}(\dot{\boldsymbol{q}})$ is a vector of frictional forces, $\boldsymbol{E}(\boldsymbol{q})$ is the input transformation matrix, $\boldsymbol{\tau}$ is the torque vector, and $\boldsymbol{\lambda}$ is the vector of constraint forces [4].

Deriving the WMR dynamics, requires the elimination of the kinematic constraints $\boldsymbol{A}^T(\boldsymbol{q})\boldsymbol{\lambda}$ from (2). In literature [4], [6], [8], this is done by differentiating (1) with respect to time, substituting the expression for $\ddot{\boldsymbol{q}}$ in (2), pre-multiplying the resulting expression by $\boldsymbol{S}^T(\boldsymbol{q})$, and noting that $\boldsymbol{S}^T(\boldsymbol{q})\boldsymbol{A}^T(\boldsymbol{q}) = \boldsymbol{0}$. The resulting dynamic model is given by

$$\bar{\boldsymbol{M}}\dot{\boldsymbol{\nu}} + \bar{\boldsymbol{V}}(\dot{\boldsymbol{q}})\boldsymbol{\nu} + \bar{\boldsymbol{F}}(\dot{\boldsymbol{q}}) = \boldsymbol{\tau}, \tag{3}$$

where:

$$\bar{\boldsymbol{M}} = \begin{bmatrix} \frac{r^2}{4b^2}(mb^2+I)+I_w & \frac{r^2}{4b^2}(mb^2-I) \\ \frac{r^2}{4b^2}(mb^2-I) & \frac{r^2}{4b^2}(mb^2+I)+I_w \end{bmatrix},$$

$$\bar{\boldsymbol{V}}(\dot{\boldsymbol{q}}) = \begin{bmatrix} 0 & \frac{m_c r^2 d\dot{\phi}}{2b} \\ \frac{m_c r^2 d\dot{\phi}}{2b} & 0 \end{bmatrix},$$

$\bar{\boldsymbol{F}}(\dot{\boldsymbol{q}}) = \boldsymbol{S}^T(\boldsymbol{q})\boldsymbol{F}(\dot{\boldsymbol{q}})$, $I = (I_c + m_c d^2) + 2(I_m + m_w b^2)$, and $m = m_c + 2m_w$. It is important to note that:

Remark 2.1: $\bar{\boldsymbol{M}}$ is symmetric, positive definite, and is independent of the state vector or its derivatives.

Remark 2.2: $\bar{\boldsymbol{V}}(\dot{\boldsymbol{q}})$ and $\bar{\boldsymbol{F}}(\dot{\boldsymbol{q}})$ constitute the nonlinear terms in the WMR dynamics.

Remark 2.3: $\bar{\boldsymbol{V}}(\dot{\boldsymbol{q}})$ is effectively a function of $\boldsymbol{\nu}$, since $\dot{\phi} = \frac{r}{2b}(\nu_r - \nu_l)$ as can be seen in (1).

To account for the fact that the controller is to be implemented on a digital computer, the continuous-time dynamics (3) are discretized through a first order forward Euler approximation with a sampling interval of T seconds. The resulting nonlinear discrete-time dynamic model is given by

$$\boldsymbol{\nu}_k - \boldsymbol{\nu}_{k-1} = \boldsymbol{f}_{k-1} + \boldsymbol{G}_{k-1}\boldsymbol{\tau}_{k-1}, \tag{4}$$

where the subscript integer k denotes that the corresponding variable is evaluated at time kT seconds, and vector $\boldsymbol{f}_{k-1}$ and matrix $\boldsymbol{G}_{k-1}$, which together encapsulate the WMR dynamics, are given by

$$\begin{aligned} \boldsymbol{f}_{k-1} &= -T\bar{\boldsymbol{M}}_{k-1}^{-1}\left(\bar{\boldsymbol{V}}_{k-1}\boldsymbol{\nu}_{k-1} + \bar{\boldsymbol{F}}_{k-1}\right), \\ \boldsymbol{G}_{k-1} &= T\bar{\boldsymbol{M}}_{k-1}^{-1}. \end{aligned}$$

The following conditions are assumed to hold:

Assumption 2.1: The control input vector $\boldsymbol{\tau}$ remains constant over a sampling interval of T seconds (zero order hold).

Assumption 2.2: The sampling interval is chosen low enough for the Euler approximation error to be negligible.

III. Control Design

The trajectory tracking task of WMRs is commonly defined via the concept of the *virtual vehicle* [2]. The time dependent reference trajectory is designated by a non-stationary virtual vehicle, kinematically identical to the real robot. The controller aims for the real WMR to track the virtual vehicle at all times, in both pose and velocity, by minimising the discrete-time tracking error vector $\boldsymbol{e}_k$ defined as

$$\boldsymbol{e}_k \triangleq \begin{bmatrix} e_{1_k} \\ e_{2_k} \\ e_{3_k} \end{bmatrix} \triangleq \begin{bmatrix} \cos\phi_k & \sin\phi_k & 0 \\ -\sin\phi_k & \cos\phi_k & 0 \\ 0 & 0 & 1 \end{bmatrix} (\boldsymbol{p_r}_k - \boldsymbol{p}_k), \tag{5}$$

where $\boldsymbol{p_r}_k \triangleq [x_{rk} \quad y_{rk} \quad \phi_{rk}]^T$ denotes the virtual vehicle pose vector at sampling instant k.

A. Kinematic Control

In trajectory tracking, the objective is to make $\boldsymbol{e}$ converge to zero, so that $\boldsymbol{p}$ converges to $\boldsymbol{p_r}$. For this task, a discrete-time version of the continuous-time kinematic controller originally presented in [2] is employed. This is given by

$$\boldsymbol{\nu_c}_k = \boldsymbol{C} \begin{bmatrix} v_{rk}\cos e_{3k} + k_1 e_{1k} \\ \omega_{rk} + k_2 v_{rk} e_{2k} + k_3 v_{rk} \sin e_{3k} \end{bmatrix}, \tag{6}$$

where $\boldsymbol{\nu_c}_k$ is the wheel velocity command vector issued by the kinematic controller, k_1, k_2, and k_3 are *positive* design parameters, v_{rk} and ω_{rk} are the translational and angular virtual vehicle velocities respectively, and $\boldsymbol{C}$ is a velocity conversion matrix given by

$$\boldsymbol{C} = \begin{bmatrix} \frac{1}{r} & \frac{b}{r} \\ \frac{1}{r} & -\frac{b}{r} \end{bmatrix}.$$

If one assumes perfect velocity tracking (i.e. $\boldsymbol{\nu}_k = \boldsymbol{\nu_c}_k \quad \forall \quad k$), and ignores the WMR dynamic effects by considering only the kinematic model (1), then (6) completely solves the trajectory tracking problem. However as mentioned earlier, mere kinematic control rarely suffices, and often leads to performance degradation in demanding practical control situations where dynamic effects are no longer negligible [6], [10].

B. Nonadaptive Dynamic Control

If the nonlinear dynamic functions $\boldsymbol{f}_k$ and $\boldsymbol{G}_k$ are perfectly known, the control law

$$\boldsymbol{\tau}_k = \boldsymbol{G}_k^{-1}\left(\boldsymbol{\nu}_{\boldsymbol{c}k+1} - \boldsymbol{\nu}_k - \boldsymbol{f}_k + k_d\left(\boldsymbol{\nu}_{\boldsymbol{c}k} - \boldsymbol{\nu}_k\right)\right), \tag{7}$$

with the design parameter $-1 < k_d < 1$, yields the following closed-loop dynamics

$$\boldsymbol{\nu}_{k+1} = \boldsymbol{\nu}_{\boldsymbol{c}k+1} + k_d\left(\boldsymbol{\nu}_{\boldsymbol{c}k} - \boldsymbol{\nu}_k\right). \tag{8}$$

Note that in contrast to [7], [11], [43], the proposed control law (7) has the desirable property of yielding closed loop dynamics which are completely independent of the robot parameters. Moreover, this control law solves the velocity tracking problem, since (8) and the choice of k_d assure that $|\boldsymbol{\nu}_{\boldsymbol{c}k} - \boldsymbol{\nu}_k| \to 0$ as $k \to \infty$. It is important to note the issues presented in the following remarks:

Remark 3.1: Control law (7) requires the velocity command vector $\boldsymbol{\nu}_{\boldsymbol{c}k+1}$ to be available at instant k. For this reason, the kinematic control law (6) is advanced by one sampling interval. This means that at instant k, the values of v_{rk+1}, ω_{rk+1} and $\boldsymbol{e}_{k+1}$ need to be known. Additionally, from (5) it is clear that $\boldsymbol{p}_{\boldsymbol{r}k+1}$ and $\boldsymbol{p}_{k+1}$ are also required to determine $\boldsymbol{e}_{k+1}$. Having the values of $\boldsymbol{p}_{\boldsymbol{r}k+1}$, v_{rk+1} and ω_{rk+1} available at instant k is easy, since it simply means that the path-planning algorithm is required to generate the reference trajectory one sampling interval ahead. On the other hand, we propose to estimate the value of $\boldsymbol{p}_{k+1}$ via the first-order approximation $\boldsymbol{p}_{k+1} \approx 2\boldsymbol{p}_k - \boldsymbol{p}_{k-1}$. This is justified because it assumes that a typical sampling interval in the order of milliseconds, is short enough to reasonably consider $\dot{\boldsymbol{p}}$ to remain constant between two consecutive samples.

Remark 3.2: The case with $k_d = 0$ in (7), corresponds to *deadbeat control* associated with digital control systems [44].

C. Dual Adaptive Dynamic Control

The dynamic control law (7) driven by the kinematic law (6), solves the trajectory tracking problem when the WMR dynamic functions $\boldsymbol{f}_{k-1}$ and $\boldsymbol{G}_{k-1}$ in (4) are completely known. As emphasized in Section I, this is rarely the case in real-life robotic applications commonly manifesting: unmodelled dynamics, unknown/time-varying parameters, and imperfect/noisy sensor measurements. In previous publications [15], [16], we tackle these issues via HCE adaptive

control. In contrast, the two schemes presented in this paper not only consider $\boldsymbol{f}_{k-1}$ and $\boldsymbol{G}_{k-1}$ to be completely unknown, but also feature dual adaptive properties to handle the issue of uncertainty as explained in Section I.

1) GaRBF Dual Adaptive Scheme: Within this scheme, a GaRBF ANN [45] is used to approximate the vector of discrete nonlinear functions $\boldsymbol{f}_{k-1}$. The advantage of using a GaRBF ANN comes from the fact that the unknown optimal parameters appear linearly in the neural network equations. This detail, which is clarified further in the following treatment, permits the use of the well established techniques of Kalman filtering for the real-time, least-squares-sense optimal estimation of the unknown neural network parameters.

The GaRBF ANN employed to approximate $\boldsymbol{f}_{k-1}$, the estimate of which is denoted by $\hat{\boldsymbol{f}}_{k-1}$, is given by

$$\hat{\boldsymbol{f}}_{k-1} = \begin{bmatrix} \boldsymbol{\phi}^T(\boldsymbol{x}_{k-1})\hat{\boldsymbol{w}}_{\mathbf{1}k} \\ \boldsymbol{\phi}^T(\boldsymbol{x}_{k-1})\hat{\boldsymbol{w}}_{\mathbf{2}k} \end{bmatrix}, \tag{9}$$

in the light of the following definitions and assumptions:

Definition 3.1: $\boldsymbol{x}_{k-1}$ represents the ANN input vector, which in this case is set to $\boldsymbol{\nu}_{k-1}$.

Definition 3.2: $\boldsymbol{\phi}(\boldsymbol{x})$ is the ANN Gaussian basis function vector, whose ith element is given by

$$\phi_i = \exp\left(-0.5 \times (\boldsymbol{x} - \boldsymbol{m_i})^T \boldsymbol{R_r}^{-1} (\boldsymbol{x} - \boldsymbol{m_i})\right),$$

where $\boldsymbol{m_i}$ is the centre-coordinate vector of the ith basis function, $\boldsymbol{R_r}$ is the corresponding covariance matrix, and the time index has been dropped for clarity.

Definition 3.3: $\hat{\boldsymbol{w}}_{\boldsymbol{j}_k}$ represents the weight vector of the connection between the basis functions and the jth output element of the network. The $\hat{}$ notation is used to indicate that the operand is undergoing estimation. This convention is adopted throughout the paper.

Definition 3.4: Let L denote the number of basis functions.

Assumption 3.1: The ANN input vector $\boldsymbol{x}_{k-1}$ is assumed to be contained within an arbitrarily large compact set $\boldsymbol{\chi} \subset \mathbb{R}^2$.

Assumption 3.2: The basis functions are shaped and placed within the compact set $\boldsymbol{\chi}$, by setting $\boldsymbol{m_i}$ and $\boldsymbol{R_r}$ accordingly.

Sanner and Slotine [46] show that by utilising knowledge on the frequency characteristics of the function being estimated, the number of basis functions and their corresponding means and covariance matrices can be selected so as to satisfy a desired level of optimal approximation

error. Moreover, our simulations indicate that the overall performance of the controller is not overly sensitive to the placement and covariance of the basis functions as long as Assumption 3.1 is adhered to.

From Remark 2.1 it follows that $\boldsymbol{G}_{k-1}$ has the following form

$$\boldsymbol{G}_{k-1} = \begin{bmatrix} g_{1k-1} & g_{2k-1} \\ g_{2k-1} & g_{1k-1} \end{bmatrix},$$

a symmetric state-independent matrix, with unknown elements. Consequently, its estimation does not require the use of an ANN. The symmetry of $\boldsymbol{G}_{k-1}$ is exploited when constructing its estimate $\hat{\boldsymbol{G}}_{k-1}$ by imposing the following structure

$$\hat{\boldsymbol{G}}_{k-1} = \begin{bmatrix} \hat{g}_{1k-1} & \hat{g}_{2k-1} \\ \hat{g}_{2k-1} & \hat{g}_{1k-1} \end{bmatrix}, \tag{10}$$

where $\hat{g}_{1k-1}$ and $\hat{g}_{2k-1}$ represent the estimates of the unknown elements g_{1k-1} and g_{2k-1}.

The GaRBF ANN parameter-tuning algorithm is developed next. Some definitions and assumptions are required before proceeding:

Definition 3.5:

$$\boldsymbol{\Phi}_{k-1} \triangleq \begin{bmatrix} \boldsymbol{\phi}^T & \mathbf{0}^T \\ \mathbf{0}^T & \boldsymbol{\phi}^T \end{bmatrix}, \quad \boldsymbol{\Gamma}_{k-1} \triangleq \begin{bmatrix} \tau_{rk-1} & \tau_{lk-1} \\ \tau_{lk-1} & \tau_{rk-1} \end{bmatrix},$$

and $\boldsymbol{H}_{k-1} \triangleq [\boldsymbol{\Phi}_{k-1} \ \vdots \ \boldsymbol{\Gamma}_{k-1}]$, where: $\mathbf{0}$ is a zero vector bearing the same length as $\boldsymbol{\phi}$, τ_{rk-1} and τ_{lk-1} are the first and second elements of the torque vector $\boldsymbol{\tau}_{k-1}$ respectively, and the time index in $\boldsymbol{\Phi}_{k-1}$ indicates that $\boldsymbol{\phi}$ is a function of $\boldsymbol{x}_{k-1}$.

Definition 3.6: The individual parameter vectors requiring estimation, are all grouped into a single vector $\hat{\boldsymbol{z}}_k \triangleq [\hat{\boldsymbol{w}}_{\mathbf{1}k}^T \ \ \hat{\boldsymbol{w}}_{\mathbf{2}k}^T \ \ \hat{g}_{1k-1} \ \ \hat{g}_{2k-1}]^T$.

Definition 3.7: The measured output in the dynamic model (4) is denoted by $\boldsymbol{y}_k \triangleq \boldsymbol{\nu}_k - \boldsymbol{\nu}_{k-1}$.

Definition 3.8: The *information state* [25], denoted by I^k, consists of all output measurements up to instant k and all the previous inputs, denoted by Y^k and U^{k-1} respectively.

Assumption 3.3: Inside the compact set $\boldsymbol{\chi}$, the ANN approximation error is negligibly small, when the synaptic weight vectors $\hat{\boldsymbol{w}}_{\mathbf{1}k}$ and $\hat{\boldsymbol{w}}_{\mathbf{2}k}$, are equal to some unknown optimal vectors denoted by $\boldsymbol{w}_{\mathbf{1}k}^*$ and $\boldsymbol{w}_{\mathbf{2}k}^*$ respectively.

This assumption is justified in the light of the *Universal Approximation Theorem* of neural networks [45]. The * notation is used throughout the paper to refer to the optimal value of the operand. In view of the stochastic adaptive approach taken in this paper, the unknown optimal parameter vector $\boldsymbol{z}_k^* \triangleq [\boldsymbol{w}_{1k}^{*T} \;\; \boldsymbol{w}_{2k}^{*T} \;\; g_{1k-1} \;\; g_{2k-1}]^T$ is treated as a random variable. In the following we assume that the initial value of $\boldsymbol{z}_k^*$ has a Gaussian distribution.

Assumption 3.4: $p(\boldsymbol{z}_0^*) \sim \mathcal{N}(\bar{\boldsymbol{z}}_0, \boldsymbol{R}_{\boldsymbol{z}0})$.

In practice, $\boldsymbol{R}_{\boldsymbol{z}0}$ reflects the confidence in prior knowledge of the estimated vector; larger values indicating less confidence in the initial parameter estimate vector $\bar{\boldsymbol{z}}_0$.

The stochastic formulation of this problem can also include, in a straight forward manner, uncertainty in the measurements (e.g. due to noisy sensors). We therefore introduce a discrete random vector $\boldsymbol{\epsilon}_k$ additively with the measured output $\boldsymbol{y}_k$ under the following assumptions:

Assumption 3.5: $\boldsymbol{\epsilon}_k$ is an independent zero-mean white Gaussian process, with covariance matrix $\boldsymbol{R}_{\boldsymbol{\epsilon}}$.

Assumption 3.6: $\boldsymbol{z}_0^*$ and $\boldsymbol{\epsilon}_k$ are mutually independent $\forall k$.

By (9), (10), Definitions 3.1 to 3.7, and Assumptions 3.1 to 3.3, it follows that the WMR dynamic model (4) can be represented in the following state-space form

$$\begin{aligned} \boldsymbol{z}_{k+1}^* &= \boldsymbol{z}_k^* \\ \boldsymbol{y}_k &= \boldsymbol{H}_{k-1}\boldsymbol{z}_k^* + \boldsymbol{\epsilon}_k. \end{aligned} \tag{11}$$

As seen in 11, the GaRBF ANN leads to a model which is linear in terms of the unknown neural network parameters. This is exploited by employing the well known Kalman filter [47] in predictive mode, for the real-time least-square sense optimal stochastic estimation of $\boldsymbol{z}_{k+1}^*$, as detailed in the following lemma.

Lemma 3.1: In the light of all the previous definitions, Assumptions 3.4 to 3.6 and (11), it follows that $p(\boldsymbol{z}_{k+1}^*|I^k) \sim \mathcal{N}(\hat{\boldsymbol{z}}_{k+1}, \boldsymbol{P}_{k+1})$, and so $\hat{\boldsymbol{z}}_{k+1}$ is the optimal estimate of $\boldsymbol{z}_{k+1}^*$ conditioned on I^k, provided that $\hat{\boldsymbol{z}}_{k+1}$ and $\boldsymbol{P}_{k+1}$ satisfy the following Kalman filter equations:

$$\begin{aligned} \hat{\boldsymbol{z}}_{k+1} &= \hat{\boldsymbol{z}}_k + \boldsymbol{K}_k\boldsymbol{i}_k \\ \boldsymbol{P}_{k+1} &= \boldsymbol{P}_k - \boldsymbol{K}_k\boldsymbol{H}_{k-1}\boldsymbol{P}_k, \end{aligned} \tag{12}$$

where the Kalman gain matrix, the innovations vector, and the filter's initial conditions are respectively given by:

$\boldsymbol{K}_k = \boldsymbol{P}_k \boldsymbol{H}_{k-1}^T \left(\boldsymbol{H}_{k-1} \boldsymbol{P}_k \boldsymbol{H}_{k-1}^T + \boldsymbol{R}_{\boldsymbol{\epsilon}} \right)^{-1}$, $\boldsymbol{i}_k = \boldsymbol{y}_k - \boldsymbol{H}_{k-1} \hat{\boldsymbol{z}}_k$, and $\hat{\boldsymbol{z}}_0 = \bar{\boldsymbol{z}}_0$, $\boldsymbol{P}_0 = \boldsymbol{R}_{\boldsymbol{z}0}$. Additionally, in the light of (11), (12), Definition 3.8, and the theory of Gaussian random variables [48], it follows that $p(\boldsymbol{y}_{k+1}|I^k) \sim \mathcal{N}(\boldsymbol{H}_k \hat{\boldsymbol{z}}_{k+1}, \boldsymbol{H}_k \boldsymbol{P}_{k+1} \boldsymbol{H}_k^T + \boldsymbol{R}_{\boldsymbol{\epsilon}})$.

Proof: The proof follows directly that of the standard predictive type Kalman filter [47], [48] when applied to the state-space stochastic model (11). ■

The Kalman filter formulation (12) constitutes the adaptation law for the proposed GaRBF dual adaptive scheme. Additionally, it provides a real-time update of the density $p(\boldsymbol{y}_{k+1}|I^k)$. This information is essential in dual control since unlike HCE schemes, the uncertainty of the estimates is not ignored.

The dual control law for the GaRBF scheme is presented next. It is based on the innovations dual method originally proposed by Milito *et. al.* [37] for SISO linear systems. This approach was later extended by Fabri and Kadirkamanathan [25], [34] for dual adaptive neural control of nonlinear SISO systems. In contrast to these works, our control law addresses the nonlinear MIMO nature of the relatively more complex WMR system.

The explicit-type suboptimal innovation-based performance index J_{inn}, adopted from [34], but modified to fit the MIMO scenario at hand is defined as

$$J_{inn} \triangleq E\Big\{ \left(\boldsymbol{y}_{k+1} - \boldsymbol{y}_{\boldsymbol{d}k+1} \right)^T \boldsymbol{Q_1} \left(\boldsymbol{y}_{k+1} - \boldsymbol{y}_{\boldsymbol{d}k+1} \right) + \left(\boldsymbol{\tau}_k^T \boldsymbol{Q_2} \boldsymbol{\tau}_k \right) + \left(\boldsymbol{i}_{k+1}^T \boldsymbol{Q_3} \boldsymbol{i}_{k+1} \right) \Big| I^k \Big\},$$

where $E\left\{ \cdot | I^k \right\}$ denotes the mathematical expectation conditioned on I^k, and the following definitions apply:

Definition 3.9: $\boldsymbol{y}_{\boldsymbol{d}k+1}$ is the reference vector of $\boldsymbol{y}_{k+1}$ and is given by $\boldsymbol{y}_{\boldsymbol{d}_{k+1}} \triangleq \boldsymbol{\nu}_{\boldsymbol{c}_{k+1}} - \boldsymbol{\nu}_k$ (refer to Definition 3.7).

Definition 3.10: Design parameters $\boldsymbol{Q_1}$, $\boldsymbol{Q_2}$ and $\boldsymbol{Q_3}$ are diagonal and $\in \mathbb{R}^{2\times 2}$. Additionally: $\boldsymbol{Q_1}$ is positive definite, $\boldsymbol{Q_2}$ is positive semi-definite, and each element of $\boldsymbol{Q_3}$ is less than or equal to 0, and greater than or equal to the corresponding element of $-\boldsymbol{Q_1}$.

Remark 3.3: The design parameter $\boldsymbol{Q_1}$ is introduced to penalize tracking errors, $\boldsymbol{Q_2}$ induces a penalty on large control inputs and prevents ill-conditioning, and $\boldsymbol{Q_3}$ affects the innovation vector so as to induce the dual adaptive feature characterising this work.

The dual adaptive control law proposed for this scheme is stated by the following theorem.

Theorem 3.1: The control law minimising performance index J_{inn} (13), subject to the WMR

dynamic model (4) and all previous definitions, assumptions and Lemma 3.1, is given by

$$\boldsymbol{\tau}_k = \left(\hat{\boldsymbol{G}}_k^T \boldsymbol{Q_1} \hat{\boldsymbol{G}}_k + \boldsymbol{Q_2} + \boldsymbol{N}_{k+1}\right)^{-1} \times \left(\hat{\boldsymbol{G}}_k^T \boldsymbol{Q_1}\left(\boldsymbol{y_{d}}_{k+1} - \hat{\boldsymbol{f}}_k\right) - \boldsymbol{\kappa}_{k+1}\right), \tag{13}$$

where the following definitions apply:

Definition 3.11: Let $\boldsymbol{Q_4} \triangleq \boldsymbol{Q_1} + \boldsymbol{Q_3}$, and the i^{th} row, j^{th} column element of any matrix $\boldsymbol{A_S}$ be denoted by $a_S(i,j)$.

Definition 3.12: $\boldsymbol{P}_{k+1}$ in (12) is repartitioned as

$$\boldsymbol{P}_{k+1} = \begin{bmatrix} \boldsymbol{P_{ff}}_{k+1} & \boldsymbol{P_{Gf}}_{k+1}^T \\ \boldsymbol{P_{Gf}}_{k+1} & \boldsymbol{P_{GG}}_{k+1} \end{bmatrix},$$

where: $\boldsymbol{P_{ff}}_{k+1} \in \mathbb{R}^{2L \times 2L}$ and $\boldsymbol{P_{GG}}_{k+1} \in \mathbb{R}^{2\times 2}$.

Definition 3.13: Auxiliary matrix $\boldsymbol{B} \triangleq \boldsymbol{P_{Gf}}_{k+1} \boldsymbol{\Phi}_k^T \boldsymbol{Q_4}$, and $\boldsymbol{\kappa}_{k+1} \triangleq \begin{bmatrix} b(1,1)+b(2,2) & b(1,2)+b(2,1) \end{bmatrix}^T$.

Definition 3.14: The elements of $\boldsymbol{N}_{k+1}$ are given by:

$$\begin{aligned} n(1,1) &= q_4(1,1)p_{GG}(1,1) + q_4(2,2)p_{GG}(2,2) \\ n(2,2) &= q_4(1,1)p_{GG}(2,2) + q_4(2,2)p_{GG}(1,1) \\ n(1,2) &= 0.5 \times \Big(q_4(1,1)p_{GG}(1,2) + q_4(1,1)p_{GG}(2,1) \\ &\quad + q_4(2,2)p_{GG}(1,2) + q_4(2,2)p_{GG}(2,1)\Big) \\ n(2,1) &= n(1,2). \end{aligned}$$

Note that the time index in $\boldsymbol{N}_{k+1}$ indicates that each individual element $p_{GG}(\cdot,\cdot)$ corresponds to $\boldsymbol{P_{GG}}_{k+1}$.

Proof: By the Gaussian distribution of $p(\boldsymbol{y}_{k+1}|I^k)$ specified in Lemma 3.1, and standard results from multivariate probability theory, it follows that cost function (13) can be written as

$$\begin{aligned} J_{inn} &= \left(\boldsymbol{H}_k \hat{\boldsymbol{z}}_{k+1} - \boldsymbol{y_{d}}_{k+1}\right)^T \boldsymbol{Q_1} \left(\boldsymbol{H}_k \hat{\boldsymbol{z}}_{k+1} - \boldsymbol{y_{d}}_{k+1}\right) \\ &+ trace\left\{\boldsymbol{Q_4}\left(\boldsymbol{H}_k \boldsymbol{P}_{k+1} \boldsymbol{H}_k^T + \boldsymbol{R_\epsilon}\right)\right\} + \boldsymbol{\tau}_k^T \boldsymbol{Q_2} \boldsymbol{\tau}_k. \end{aligned}$$

By replacing $\boldsymbol{H}_k \hat{\boldsymbol{z}}_{k+1}$ by $\hat{\boldsymbol{f}}_k + \hat{\boldsymbol{G}}_k \boldsymbol{\tau}_k$, and employing the formulations in Definitions 3.5 and 3.12 to factorize completely the resulting expression in terms of $\boldsymbol{\tau}_k$, it is possible to differentiate the cost function with respect to $\boldsymbol{\tau}_k$ and equate to zero, in order to get the dual control law (13). The

resulting second order partial derivative of J_{inn} with respect to $\boldsymbol{\tau}_k$, the Hessian matrix, is given by $2 \times \left(\hat{\boldsymbol{G}}_k^T \boldsymbol{Q_1} \hat{\boldsymbol{G}}_k + \boldsymbol{Q_2} + \boldsymbol{N}_{k+1}\right)$. By Definitions 3.10 and 3.14, it is clear that the Hessian matrix is positive definite, meaning that $\boldsymbol{\tau}_k$ in (13) minimizes the dual performance index (13) uniquely. Moreover, the latter implies that the inverse term in (13) exists without exceptions. ■ Referring to control law (13) one can note the following:

Remark 3.4: $\boldsymbol{Q_3}$ which appears in (13) via $\boldsymbol{\kappa}_{k+1}$ acts as a weighting factor, where at one extreme, with $\boldsymbol{Q_3} = -\boldsymbol{Q_1}$, the controller completely ignores the estimates' uncertainty, resulting in HCE control, and at the other extreme, with $\boldsymbol{Q_3} = \boldsymbol{0}$, it gives maximum attention to uncertainty, which leads to *cautious control*. For intermediate settings of $\boldsymbol{Q_3}$, the controller strikes a compromise and operates in dual adaptive mode. It is well known that HCE control leads to large tracking errors and excessive control actions when the estimates' uncertainty is relatively high. On the other hand, cautious control is notorious for sluggish response and *control turn-off* [25], [29]. Consequently, dual control exhibits superior performance by striking a balance between the two extremes.

2) Sigmoidal MLP Dual Adaptive Scheme: Another type of neural network, commonly employed in control applications, is the sigmoidal MLP ANN [7], [14], [16], [45]. Unfortunately, MLP networks do not preserve the desirable property of linearity in the unknown network parameters exhibited by radial basis function networks. As a result, the former Kalman filter has to be replaced by a suboptimal, nonlinear, stochastic estimator, like the extended Kalman filter (EKF), which complicates the derivation of the control law and introduces certain approximations. On the other hand, unlike the activation functions employed in GaRBF ANNs, the sigmoidal functions in MLPs do not have localized receptive fields, implying that typically MLP networks require less neurons than GaRBF ANNs to achieve the same degree of accuracy. This implies that MLPs tend to be less computationally demanding, making them attractive for high-order systems, since the number of neurons need not rise exponentially with the number of states; a well known effect known as the *curse of dimensionality* [49].

Within this scheme, a sigmoidal MLP ANN with one hidden layer is used to approximate the unknown vector $\boldsymbol{f}_{k-1}$. Consequently, a new parameter-tuning algorithm and control law, differing from those of the GaRBF scheme, need to be derived. In the following treatment some of the variables defined earlier within the previous scheme are redefined and reused. Hence each variable, definition, assumption or remark, should be interpreted in the context of the scheme in

focus at the time.

The sigmoidal MLP ANN output is given by

$$\hat{\boldsymbol{f}}_{k-1} = \begin{bmatrix} \boldsymbol{\phi}^T(\boldsymbol{x}_{k-1}, \hat{\boldsymbol{a}}_k)\hat{\boldsymbol{w}}_{\mathbf{1}k} \\ \boldsymbol{\phi}^T(\boldsymbol{x}_{k-1}, \hat{\boldsymbol{a}}_k)\hat{\boldsymbol{w}}_{\mathbf{2}k} \end{bmatrix}, \tag{14}$$

where the following definitions are in order:

Definition 3.15: $\boldsymbol{x}_{k-1} \triangleq [\boldsymbol{\nu}_{k-1} \quad 1]$ is the ANN input, where the augmented constant serves as a bias input.

Definition 3.16: $\boldsymbol{\phi}(\cdot,\cdot)$ is the vector of sigmoidal activation functions, whose ith element is given by

$\phi_i = \left(1 + \exp(-\hat{\boldsymbol{s}_i}^T \boldsymbol{x})\right)^{-1}$, where $\hat{\boldsymbol{s}_i}$ is ith vector element in the group vector $\hat{\boldsymbol{a}}$;

i.e. $\hat{\boldsymbol{a}} \triangleq \left[\hat{\boldsymbol{s}_1}^T \cdots \hat{\boldsymbol{s}_L}^T\right]^T$, where L denotes the number of neurons. In practice $\hat{\boldsymbol{s}_i}$ characterizes the shape of the ith neuron.

In this definition, the time index has been dropped for the sake of clarity.

Definition 3.17: $\hat{\boldsymbol{w}}_{\boldsymbol{j}_k}$ represents the synaptic weight estimate vector of the connection between the neurons in the hidden hidden layer and the jth output element of the ANN.

The sigmoidal MLP ANN parameter-tuning algorithm is developed next. The following formulation is required.

Definition 3.18: The unknown network parameters requiring estimation are grouped in a single vector

$\hat{\boldsymbol{z}}_k \triangleq \left[\hat{\boldsymbol{r}}_k^T \quad \hat{\boldsymbol{g}}_k^T\right]^T$, where $\hat{\boldsymbol{r}}_k \triangleq \left[\hat{\boldsymbol{w}}_{\mathbf{1}k}^T \quad \hat{\boldsymbol{w}}_{\mathbf{2}k}^T \quad \hat{\boldsymbol{a}}_k^T\right]^T$ and $\hat{\boldsymbol{g}}_k \triangleq \left[\hat{g}_{1k-1} \quad \hat{g}_{2k-1}\right]$. The latter vector groups up the elements of $\hat{\boldsymbol{G}}_{k-1}$, as defined in (10).

Assumption 3.7: Inside the compact set $\boldsymbol{\chi}$, the neural network approximation error is negligibly small when the ANN parameter vector $\hat{\boldsymbol{r}}_k$ is equal to some unknown optimal vector denoted by $\boldsymbol{r}_k^*$.

The latter follows the same justification as in the case of Assumption 3.3.

By (10) and (14), Definitions 3.7, and 3.15 to 3.18, and Assumptions 3.1, 3.5 and 3.7, it follows that the dynamic model (4) can be represented in the following state-space form

$$\begin{aligned} \boldsymbol{z}_{k+1}^* &= \boldsymbol{z}_k^* \\ \boldsymbol{y}_k &= \boldsymbol{h}\left(\boldsymbol{x}_{k-1}, \boldsymbol{\tau}_{k-1}, \boldsymbol{z}_k^*\right) + \boldsymbol{\epsilon}_k, \end{aligned} \tag{15}$$

where $\boldsymbol{h}\left(\boldsymbol{x}_{k-1}, \boldsymbol{\tau}_{k-1}, \boldsymbol{z}_k^*\right)$ is a nonlinear vector field in terms of the unknown optimal parameter $\boldsymbol{z}_k^*$ given by,

$$\boldsymbol{h}\left(\boldsymbol{x}_{k-1}, \boldsymbol{\tau}_{k-1}, \boldsymbol{z}_k^*\right) = \hat{\boldsymbol{f}}_{k-1}(\boldsymbol{x}_{k-1}, \boldsymbol{r}_k^*) + \hat{\boldsymbol{G}}_{k-1}(\boldsymbol{g}_k^*)\boldsymbol{\tau}_{k-1}.$$

It should be noted that:

Remark 3.5: The unknown optimal parameter vector $\boldsymbol{z}_k^*$, required for the estimation of $\boldsymbol{f}_{k-1}$ and $\boldsymbol{G}_{k-1}$ in (14) and (10) respectively, does not appear linearly in the system model (15). Consequently nonlinear estimation techniques have to be used.

In this paper we opt to employ the well known EKF [48] in predictive mode for the estimation of $\boldsymbol{z}_{k+1}^*$, as detailed right after the following set of necessary preliminaries.

Definition 3.19: $\boldsymbol{\nabla}_{\boldsymbol{h}k}$ denotes the Jacobian matrix of $\boldsymbol{h}\left(\boldsymbol{x}_{k-1}, \boldsymbol{\tau}_{k-1}, \boldsymbol{z}_k^*\right)$ with respect to $\boldsymbol{z}_k^*$ evaluated at $\hat{\boldsymbol{z}}_k$.

By (10), (14), and (16) it can be shown that:

$$\boldsymbol{\nabla}_{\boldsymbol{h}k} \triangleq \left[\boldsymbol{\nabla}_{\boldsymbol{f}k} \quad \boldsymbol{\nabla}_{\boldsymbol{\Gamma}k}\right] \triangleq \left[\frac{\partial(\hat{\boldsymbol{f}}_{k-1})}{\partial(\hat{\boldsymbol{r}}_k)} \quad \frac{\partial(\hat{\boldsymbol{G}}_{k-1}\boldsymbol{\tau}_{k-1})}{\partial(\hat{\boldsymbol{g}}_k)}\right],$$

where:

$$\frac{\partial(\hat{\boldsymbol{f}}_{k-1})}{\partial(\hat{\boldsymbol{r}}_k)} = \begin{bmatrix} \boldsymbol{\phi}_{k-1}^T & \mathbf{0}^T & \cdots \hat{w_{1,i}}(\phi_i - \phi_i{}^2)\boldsymbol{x}^T \cdots \\ \mathbf{0}^T & \boldsymbol{\phi}_{k-1}^T & \cdots \hat{w_{2,i}}(\phi_i - \phi_i{}^2)\boldsymbol{x}^T \cdots \end{bmatrix},$$

$i = 1, \ \ldots \ , L$ and $\hat{w_{j,i}}$ denotes the ith element of the jth output network parameter vector $\hat{\boldsymbol{w}}_{\boldsymbol{j}k}$, notation-wise $\boldsymbol{\phi}_{k-1}$ implies that the activation function is evaluated for $\boldsymbol{x}_{k-1}$ and $\hat{\boldsymbol{a}}_k$, $\mathbf{0}$ denotes a zero vector having the same length as $\boldsymbol{\phi}_{k-1}$, and in this equation both ϕ_i and $\boldsymbol{x}$ correspond to time instant $(k-1)$;

$$\frac{\partial(\hat{\boldsymbol{G}}_{k-1}\boldsymbol{\tau}_{k-1})}{\partial(\hat{\boldsymbol{g}}_k)} = \begin{bmatrix} \tau_{rk-1} & \tau_{lk-1} \\ \\ \tau_{lk-1} & \tau_{rk-1} \end{bmatrix},$$

where $\tau_{r_{k-1}}$ and $\tau_{l_{k-1}}$ are defined in Definition (3.5).

In the light of Definitions 3.8 and 3.19, and Assumptions 3.4 and 3.6, the EKF is applied to the nonlinear stochastic model (15). The EKF effectively linearizes the non-linear function $\boldsymbol{h}\left(\boldsymbol{x}_{k-1}, \boldsymbol{\tau}_{k-1}, \boldsymbol{z}_k^*\right)$ around the current estimate $\hat{\boldsymbol{z}}_k$, and applies the Kalman filter using the resulting Jacobian and the following approximation

$$p(\boldsymbol{z}_{k+1}^* | I^k) \approx \mathcal{N}(\hat{\boldsymbol{z}}_{k+1}, \boldsymbol{P}_{k+1}), \tag{16}$$

where $\hat{\boldsymbol{z}}_{k+1}$ and $\boldsymbol{P}_{k+1}$ satisfy the EKF recursive equations

$$\begin{aligned} \hat{\boldsymbol{z}}_{k+1} &= \hat{\boldsymbol{z}}_k + \boldsymbol{K}_k \boldsymbol{i}_k, \\ \boldsymbol{P}_{k+1} &= \boldsymbol{P}_k - \boldsymbol{K}_k \boldsymbol{\nabla}_{\boldsymbol{h}k} \boldsymbol{P}_k, \end{aligned} \tag{17}$$

in which the EKF gain matrix, the innovations vector, and the filter's initial conditions are given by:
$\boldsymbol{K}_k = \boldsymbol{P}_k \boldsymbol{\nabla}_{\boldsymbol{h}_k^k}^T \left(\boldsymbol{\nabla}_{\boldsymbol{h}k} \boldsymbol{P}_k \boldsymbol{\nabla}_{\boldsymbol{h}_k^k}^T \boldsymbol{R}_{\boldsymbol{\epsilon}} \right)^{-1}$, $\boldsymbol{i}_k = \boldsymbol{y}_k - \boldsymbol{h}\left(\boldsymbol{x}_{k-1}, \boldsymbol{\tau}_{k-1}, \hat{\boldsymbol{z}}_k\right)$, and $\hat{\boldsymbol{z}}_0 = \bar{\boldsymbol{z}}_0$, $\boldsymbol{P}_0 = \boldsymbol{R}_{\boldsymbol{z}0}$ respectively.

Expressing $\boldsymbol{y}_{k+1}$ as a first order Taylor series around $\boldsymbol{z}_{k+1}^* = \hat{\boldsymbol{z}}_{k+1}$ yields the following approximation

$$\boldsymbol{y}_{k+1} \approx \boldsymbol{h}\left(\boldsymbol{x}_k, \boldsymbol{\tau}_k, \hat{\boldsymbol{z}}_{k+1}\right) + \boldsymbol{\nabla}_{\boldsymbol{h}k+1} \left(\boldsymbol{z}_{k+1}^* - \hat{\boldsymbol{z}}_{k+1} \right) + \boldsymbol{\epsilon}_{k+1}, \tag{18}$$

which results in the following lemma.

Lemma 3.2: On the basis of approximations (16) and (18), it follows that $p(\boldsymbol{y}_{k+1}|I^k)$ is approximately Gaussian with mean $\boldsymbol{h}\left(\boldsymbol{x}_k, \boldsymbol{\tau}_k, \hat{\boldsymbol{z}}_{k+1}\right)$ and covariance $\boldsymbol{\nabla}_{\boldsymbol{h}k+1} \boldsymbol{P}_{k+1} \boldsymbol{\nabla}_{\boldsymbol{h}k+1}^T + \boldsymbol{R}_{\boldsymbol{\epsilon}}$.

Proof: The proof follows directly from: the linearity of (18), the approximate conditional distribution of $\boldsymbol{z}_{k+1}^*$ in (16), and the Gaussian distribution of $\boldsymbol{\epsilon}_{k+1}$ as specified in Assumption 3.5. ■

The EKF formulation (17) constitutes the adaptation law for the proposed sigmoidal MLP dual adaptive scheme. Moreover, it provides a real-time update of the density $p(\boldsymbol{y}_{k+1}|I^k)$ as detailed in Lemma 3.2. This information is employed by the dual control law, specifically derived for this scheme, which is presented in the following theorem.

Theorem 3.2: Control law (13) minimizes the performance index used in the GaRBF scheme, namely J_{inn} (13) subject to: Definitions 3.9 and 3.10, Remark 3.3, the WMR dynamics (4), all definitions and assumptions employed within this scheme, and Lemma 3.2; in the light of Definitions 3.11 to 3.14 in the context of this scheme and subject to the following variations:

- The covariance matrix $\boldsymbol{P}_{k+1}$ is repartitioned as before according to Definition 3.12, but in this case $\boldsymbol{P}_{\boldsymbol{f}\boldsymbol{f}_{k+1}} \in \mathbb{R}^{5L \times 5L}$.
- The auxiliary matrix $\boldsymbol{B}$, in Definition 3.13, is redefined as $\boldsymbol{B} \triangleq \boldsymbol{P}_{\boldsymbol{G}\boldsymbol{f}_{k+1}} \boldsymbol{\nabla}_{\boldsymbol{f}_k^k}^T \boldsymbol{Q}_{\boldsymbol{4}}$.

Proof: Given the approximate Gaussian distribution $p(\boldsymbol{y}_{k+1}|I^k)$ in Lemma 3.2, and standard results from multivariate probability theory, it follows that within this scheme, (13) can be written

as

$$J_{inn} = \left(\boldsymbol{h}_{k+1} - \boldsymbol{y}_{\boldsymbol{d}_{k+1}}\right)^T \boldsymbol{Q_1} \left(\boldsymbol{h}_{k+1} - \boldsymbol{y}_{\boldsymbol{d}_{k+1}}\right) + \boldsymbol{\tau}_k^T \boldsymbol{Q_2} \boldsymbol{\tau}_k + \; trace \left\{ \boldsymbol{Q_4} \left(\boldsymbol{\nabla}_{\boldsymbol{h}_{k+1}} \boldsymbol{P}_{k+1} \boldsymbol{\nabla}_{\boldsymbol{h}_{k+1}}^T + \boldsymbol{R}_\epsilon \right) \right\},$$

where $\boldsymbol{h}_{k+1}$ denotes $\boldsymbol{h}\left(\boldsymbol{x}_k, \boldsymbol{\tau}_k, \hat{\boldsymbol{z}}_{k+1}\right)$. Replacing $\boldsymbol{h}_{k+1}$ by $\hat{\boldsymbol{f}}_k + \hat{\boldsymbol{G}}_k \boldsymbol{\tau}_k$ and employing the formulations in Definitions 3.12 and 3.19 to factorize completely the resulting expression in terms of $\boldsymbol{\tau}_k$, it is possible to differentiate the cost function with respect to $\boldsymbol{\tau}_k$ and equating to zero; leading to the dual control law (13) as specified in Theorem 3.2. The resulting Hessian matrix is again given by $2 \times \left(\hat{\boldsymbol{G}}_k^T \boldsymbol{Q_1} \hat{\boldsymbol{G}}_k + \boldsymbol{Q_2} + \boldsymbol{N}_{k+1} \right)$, and the same reasoning in its regards, as in the proof of Theorem 3.1, applies. ■

Remark 3.4 is also valid for the dual control law proposed for this scheme, since the latter is still based on the same innovations dual control philosophy.

IV. Simulation Results

This section presents a number of simulation results[1] demonstrating the effectiveness of the two dual control schemes proposed in this paper. Given the non-deterministic nature of the stochastic system in question, one cannot rely solely on a single simulation trial to verify the system's performance. For this reason, a comprehensive Monte Carlo comparative analysis, supported by statistical hypothesis testing, is also presented. This renders the performance evaluation process much more objective and hence reliable.

A. Simulation Scenario

Together, Equations (1) and (2) provide the continuous-time model used to simulate the differential WMR. To render the simulations more realistic, a number of model parameters, namely d, m_c, I_c and $\boldsymbol{F}(\dot{\boldsymbol{q}})$, were allowed to vary about a set of nominal values, from one simulation to another. These variations adhere to the physics of realistic randomly generated scenarios that exhibit various load configurations and surface frictional conditions. The nominal parameter values used for simulations are: $b = 0.5$m, $r = 0.15$m, $d = 0.2$m, $m_c = 30$kg, $m_w = 2$kg, $I_c = 15$kgm^2, $I_w = 0.005$kgm^2, and $I_m = 0.0025$kgm^2. Moreover, viscous friction

[1]MATLAB® was used for simulations and SPSS® for statistical testing.

was included in the model by setting $\boldsymbol{F}(\dot{\boldsymbol{q}}) = \boldsymbol{F_c}\dot{\boldsymbol{q}}$, where $\boldsymbol{F_c}$ is a diagonal matrix of coefficients, with nominal diagonal values set to $[2, 2, 5, 0.5, 0.5]$. The control sampling interval $T = 50$ms, and the additive discrete random vector $\boldsymbol{\epsilon}_k$ was set in accordance to Assumption 3.5 with covariance matrix $\boldsymbol{R_\epsilon} = 1 \times 10^{-4}\boldsymbol{I_7}$, where $\boldsymbol{I_i}$ denotes an $(i \times i)$ identity matrix.

Each simulation trial consists of seven consecutive simulations, six of which correspond to the three modes of operation (for each of the two schemes) of adaptive control law (13) namely: HCE ($\boldsymbol{Q_3} = -\boldsymbol{Q_1}$), cautious ($\boldsymbol{Q_3} = \boldsymbol{0}$) and dual ($\boldsymbol{Q_3} = -0.8\boldsymbol{Q_1}$). The remaining trials corresponds to a tuned non-adaptive (TNA) controller, which represents a non-adaptive dynamic controller implemented via (7) that assumes the model parameters to be equal to their nominal values. This is the best a non-adaptive controller can do when the exact robot parameters are unknown. In contrast, the HCE, cautious and dual controllers assume no preliminary information about the robot whatsoever, since closed loop control is activated immediately with the initial parameter estimate vector $\bar{\boldsymbol{z}}_0$ selected at random from a zero-mean, Gaussian distribution of variance 4×10^{-4}. For the sake of fair comparison, the same noise sequence, reference trajectory, initial conditions, initial filter covariance matrix ($\boldsymbol{P}_0 = 100\boldsymbol{I_\beta}$ where β is the length of vector $\hat{\boldsymbol{z}}_k$), tracking error penalty ($\boldsymbol{Q_1} = \boldsymbol{I_2}$), and control input penalty ($\boldsymbol{Q_2} = 1 \times 10^{-6}\boldsymbol{I_2}$) are used in each of the seven cases in a particular simulation trial. The noise sequence is randomly generated afresh for each trial.

B. Single Trial Analysis: GaRBF Scheme

The GaRBF ANN used for simulations contained 49 radial basis functions ($L = 49$ and $\beta = 100$) evenly placed in the two dimensional approximation region $\boldsymbol{\chi}$ ranging from -30 to 30 in steps of 10, in each dimension. It took an office desktop computer [2] with no code optimisation merely fourteen seconds to simulate one minute of real time when using the proposed GaRBF dual adaptive controller. This implies that the proposed algorithm is also computationally feasible in a practical implementation.

A number of simulation results, typifying the performance of the three control modes of the GaRBF scheme are presented in Fig. 2. Plot (a) depicts the WMR tracking a demanding reference trajectory for a non-zero initial tracking error controlled by the dual adaptive GaRBF controller.

[2]Pentium® 4 @ 3GHz, 512MB RAM.

It clearly verifies the good tracking performance of the proposed dual control scheme, even when the trajectory reaches high speeds of around 2m/s. Plots (b) to (d) correspond to one particular simulation trial. Plots (c) and (d) compare the Euclidian norm of the pose error during the transient and steady-state performance respectively. Plot (c) indicates that dual control exhibits the best transient performance among the three adaptive modes (in accordance with Remark 3.4). It is not surprising that the TNA controller leads to better initial transient response, since it requires no learning process and is pre-tuned to the nominal parameters of the actual model. However this superiority is quickly lost in the steady-state phase, depicted in Plot (d), since by that time, the initially random estimates used by the adaptive controllers would have converged to better approximates of the real functions, while the TNA controller would still be assuming the far less accurate nominal parameters that it was originally tuned with. Plot (b) depicts the Euclidian norm of the control input vector during the initial transient. The very high transient control inputs of the HCE controller reflect the aggressive and incautious nature of this controller, which ignores completely the high uncertainty in the initial estimates, and uses them as if they were perfectly true.

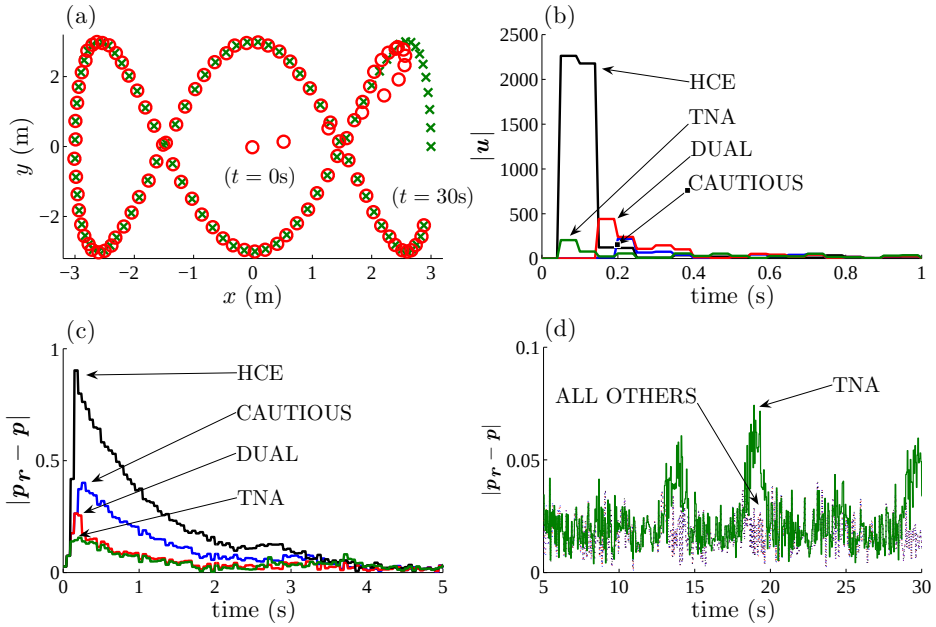

Fig. 2. (a): reference (×) & actual (◯) trajectories with GaRBF dual control; (b): control input; (c): transient tracking error; (d): steady-state tracking error.

C. Single Trial Analysis: Sigmoidal MLP Scheme

The Sigmoidal MLP ANN used for simulations contained 10 neurons ($L = 10$ and $\beta = 52$). In accordance with the comments at the end of the first paragraph in Section III-C2, it is evident that sigmoidal MLPs required less neurons than GaRBF ANNs. As a result, the simulation time for the proposed sigmoidal MLP dual adaptive controller was eight seconds per minute of real time; almost twice as fast as the GaRBF scheme.

Fig. 3 combines a number of simulation results typifying the performance of the three control modes of the sigmoidal MLP scheme. These results are very similar to those presented in Fig. 2 for the GaRBF scheme, and the same comments apply. Yet, it is incorrect to draw any conclusions regarding the overall performance of the two schemes relative to each other, based solely on the individual trial results presented so far due to the stochastic nature of the system.

D. Monte Carlo Comparative Analysis

A Monte Carlo analysis involving 1000 simulation trials was performed. Each of the seven simulations in a trial corresponds to a time horizon of three minutes in real-time under the

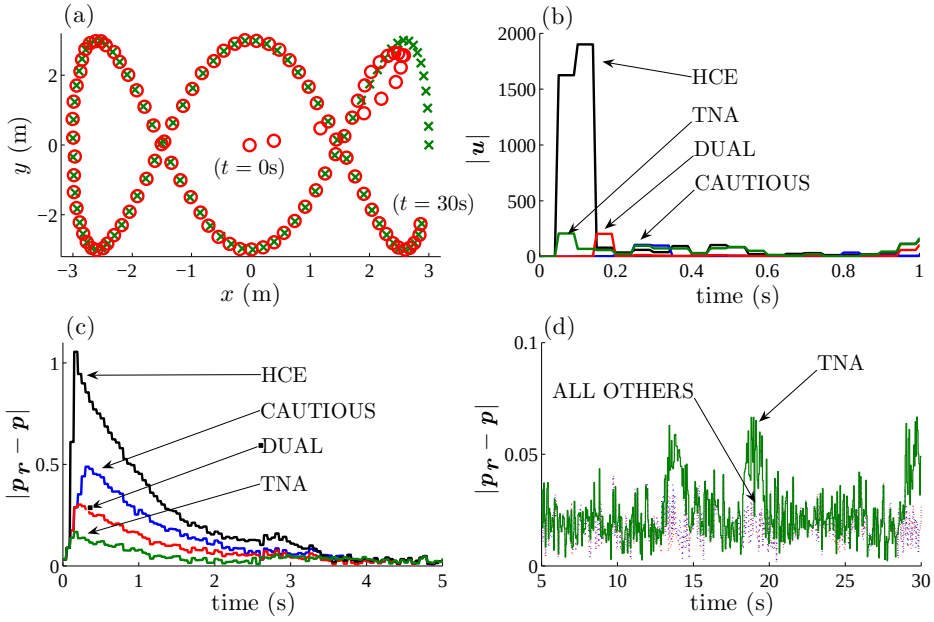

Fig. 3. (a): reference (×) & actual (◯) trajectories with MLP dual control; (b): control input; (c): transient tracking error; (d): steady-state tracking error.

simulation conditions specified earlier. After each simulation, the following cost is calculated

$$\mathcal{C}(N) = \sum_{k=1}^{N} |\boldsymbol{p_r} - \boldsymbol{p}|. \tag{19}$$

This cost is the accumulated Euclidean norm of the pose error over the whole time horizon (N sampling instants). It serves as a performance measure for each of the seven controllers operating under the same conditions, where lower values of $\mathcal{C}(N)$ are preferred.

The salient statistical features of the seven cost distributions resulting from the Monte Carlo analysis, are depicted in the boxplot of Fig. 4. Additionally, the mean and variance of each of these cost distributions are shown in Table I. These results provide the first indications of how one would rank the general performance of the seven controllers under investigation; where the dual control schemes rank best on both mean and variance. However, in order to provide a rigourous argument that the observed difference between the mean cost of each controller is statistically significant and cannot be attributed to chance, we employed a statistical inference procedure via hypothesis testing.

It is important to note that the cost distribution of the HCE GaRBF controller has a number of very high (extreme) outliers. This is the reason why the mean and variance for this controller

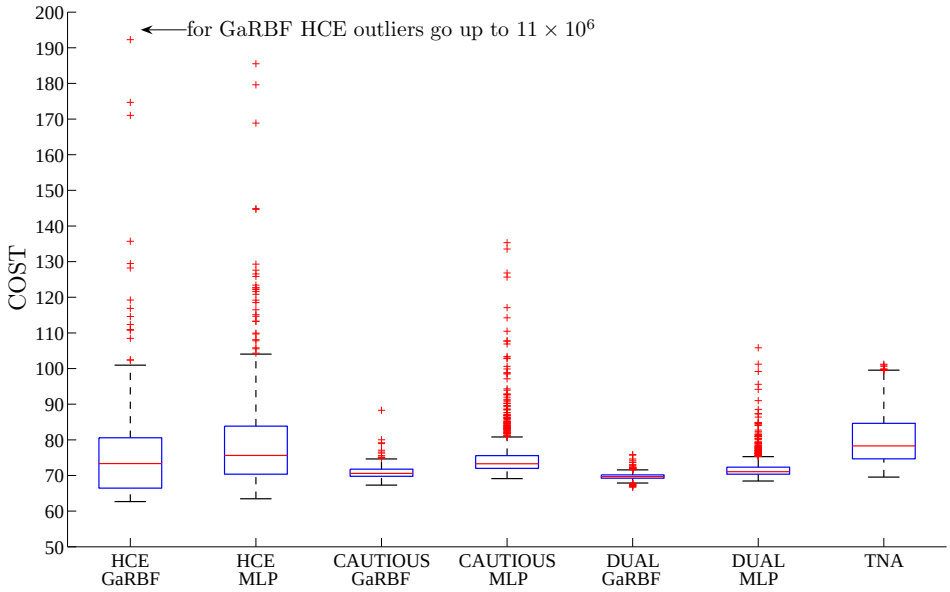

Fig. 4. Cost distributions resulting from the Monte Carlo analysis

are exceptionally high. This implies that in some cases the HCE GaRBF controller led to very high tracking errors. This is the result of the coexistence of two problems; both anticipated earlier in this paper. Specifically, the high control inputs associated with HCE control yield high robot velocities, with the possibility of the ANN input vector $(\boldsymbol{x}_{k-1} = \boldsymbol{\nu}_{k-1})$ moving well out of the highly localized GaRBF ANN approximation region $\boldsymbol{\chi}$, leading to completely erroneous approximations. For this reason the HCE GaRBF controller is withdrawn from the statistical analysis, on the basis that its behaviour, which in practice might lead to instability if left uncontrolled, is simply unacceptable and makes it unfit for further comparison.

TABLE I

MEAN AND VARIANCE OF THE COST DISTRIBUTIONS

	HCE		CAUTIOUS		DUAL		TNA
	RBF	MLP	RBF	MLP	RBF	MLP	
Mean	21094	79	71	75	70	72	80
Variance	2×10^{11}	160	2	41	1	11	55

The One-Way Analysis of Variance (ANOVA) [50] is a powerful and common statistical procedure for comparing the means of several independent samples to make inferences on their population means. It is based on the assumption that the observed data is normally distributed. The cost distributions corresponding to the six controllers left for investigation are all positively skewed (refer to Figure 4), and therefore cannot be closely approximated to normal distributions. For this reason the 1000 cost observations from each distribution were split in groups of 20 and the mean of each group calculated. In this manner a new data set composed of 50 sample means was generated for each controller. In contrast to the original cost distributions, each of the six sampling distributions of means was found to have a normal distribution. The normality assumption was verified using the Kolmogorov-Smirnov test [50]. Other graphical presentations, including Q-Q plots [50], and visual comparison of the sampling distribution (histogram) to the normal curve complemented this assumption. Statistical theory specifies that the mean of each sampling distribution is equal to the corresponding mean of the original cost distribution. Based on these results the One-Way ANOVA test was employed to compare the means of the six sampling distributions rather than the means of the six original cost distributions. The null

and alternative hypotheses for this two-tailed test are:

H_0 : In an infinite number of trials, each of the six controllers would score the same average cost as the others.

H_1 : In an infinite number of trials, two or more of the six controllers would score a different average cost from each other.

As expected, the Levene homogeneity of variance test [50] revealed that equal variances among the six data groups cannot be assumed. In such cases it is suggested that the Brown-Forsythe statistic [50] or the Welch statistic [50] is used instead of the F statistic in the One-Way ANOVA. We employed each of these three statistics in turn, and the resulting p-value [50] was always approximately zero in each case. Since the p-value was smaller than the chosen level of significance $\alpha = 0.01$, then H_0 was rejected. This implies that at least one of the six controllers is significantly better (cost-wise) than the others. In order to determine which controllers perform significantly better than which other ones, we employed the Games-Howell *post-hoc* test [50] which is highly recommended in the case of unequal variances. The results were conspicuous since all the p-values resulting from the 15 pair-wise combinations were much lower than α. This implies that the means reported in Table I are *all* significantly different and can be used to rank the performance of the six controllers. In addition to the Games-Howell test three other *post-hoc* tests, all suited for the case of unequal variances, were performed. These are: Tamhane's test, Dunnett's T3 test and Dunnett's C test [50]. Each test strongly reassured the result of the Games-Howell test. A non-parametric test using the original cost distributions instead of the sampling distributions of means, namely the Kruskal-Wallis H test [50] was also employed. The final result of this analysis reconfirmed that of the One-Way ANOVA.

With the results from the Monte Carlo comparative analysis supporting the results in Table I we can confidently claim that the proposed dual adaptive controllers (both GaRBF and MLP) bring about a significant improvement in tracking performance; not only over non-adaptive controllers which assume nominal values for the robot parameters, but also over adaptive controllers based on the HCE assumption. Moreover, it is just as evident that within each of the two schemes, the dual control mode is even better than the cautious mode, as anticipated in Remark 3.4. This complies with the dual control philosophy that a balance between *caution* and *probing* yields the best performance in adaptive control. It is also not surprising that the performance of the

GaRBF scheme is generally better than the MLP scheme. We associate the inferiority of the latter to the approximations introduced by the EKF.

V. CONCLUSIONS

The novelty in this paper comprizes the introduction of dual neuro-adaptive control for the discrete-time, dynamic control of nonholonomic mobile robots. The two proposed dual control schemes exhibit great improvements in steady-state and transient performance over non-adaptive and non-dual adaptive schemes respectively. This was confirmed by Monte Carlo simulation and a comprehensive statistical hypothesis test. Future research will investigate the replacement of the EKF in the MLP scheme, by more recent nonlinear stochastic estimators such as the unscented Kalman filter (UKF) [51]. It is envisaged that this will improve the overall performance of this scheme due to the lesser degree of approximation associated with such nonlinear estimation techniques. Additionally, it is planned to develop the work to include fault-tolerant schemes for the control of mobile robots. Early results from experiments carried out so far using a real mobile robot, confirm the same interpretation as reflected by the simulation results presented in this paper.

REFERENCES

[1] T. Tsumura, N. Fujiwara, T. Shirakawa, and M. Hashimoto, "An experimental system for automatic guidance of robot vehicle, following the route stored in memory," in *Proc. 11th International Symposium on Industrial Robots*, Oct. 1981, pp. 187–193.

[2] Y. Kanayama, Y. Kimura, F. Miyazaki, and T. Noguchi, "A stable tracking control method for an autonomous mobile robot," in *Proc. IEEE International Conference of Robotics and Automation*, Cincinnati, OH, May 1990, pp. 384–389.

[3] C. Canudas de Wit, H. Khennoul, C. Samson, and O. J. Sordalen, "Nonlinear control design for mobile robots," in *Recent Trends in Mobile Robots*, ser. Robotics and Automated Systems, Y. F. Zheng, Ed. World Scientific, 1993, ch. 5, pp. 121–156.

[4] N. Sarkar, X. Yun, and V. Kumar, "Control of mechanical systems with rolling constraints: Applications to dynamic control of mobile robots," *International Journal of Robotics Research*, vol. 13, no. 1, pp. 55–69, Feb. 1994.

[5] I. Kolmanovsky and N. H. McClamroch, "Developments in nonholonomic control problems," *IEEE Control Syst. Mag.*, vol. 15, no. 6, pp. 20–36, 1995.

[6] R. Fierro and F. L. Lewis, "Control of a nonholonomic mobile robot: Backstepping kinematics into dynamics," in *Proc. IEEE 34th Conference on Decision and Control (CDC'95)*, New Orleans, LA, Dec. 1995, pp. 3805–3810.

[7] ——, "Control of a nonholonomic mobile robot using neural networks," *IEEE Trans. Neural Netw.*, vol. 9, no. 4, pp. 589–600, Jul. 1998.

[8] T. Fukao, H. Nakagawa, and N. Adachi, "Adaptive tracking control of a nonholonomic mobile robot," *IEEE Trans. Robot. Autom.*, vol. 16, no. 5, pp. 609–615, Oct. 2000.

[9] A. D. Luca, G. Oriolo, and M. Vendittelli, "Control of wheeled mobile robots: An experimental overview," in *RAMSETE - Articulated and Mobile Robotics for Services and Technologies*, ser. Lecture Notes in Control and Information Sciences, S. Nicosia, B. Siciliano, A. Bicchi, and P. Valigi, Eds. Springer-Verlag, 2001, vol. 270, pp. 181–223.

[10] M. L. Corradini and G. Orlando, "Robust tracking control of mobile robots in the presence of uncertainties in the dynamic model," *Journal of Robotic Systems*, vol. 18, no. 6, pp. 317–323, 2001.

[11] C. de Sousa, E. M. Hemerly, and R. K. H. Galvao, "Adaptive control for mobile robot using wavelet networks," *IEEE Trans. Syst., Man, Cybern.*, vol. 32, no. 4, pp. 493–504, 2002.

[12] M. L. Corradini, G. Ippoliti, and S. Longhi, "Neural networks based control of mobile robots: Development and experimental validation," *Journal of Robotic Systems*, vol. 20, no. 10, pp. 587–600, 2003.

[13] M. Oubbati, M. Schanz, and P. Levi, "Kinematic and dynamic adaptive control of a nonholonomic mobile robot using RNN," in *Proc. IEEE Symposium on Computational Intelligence in Robotics and Automation (CIRA'05)*, Helsinki, Finland, Jun. 2005.

[14] M. K. Bugeja and S. G. Fabri, "Multilayer perceptron functional adaptive control for trajectory tracking of wheeled mobile robots," in *Proc. 2nd International Conference on Informatics in Control, Automation and Robotics (ICINCO'05)*, vol. 3, Barcelona, Spain, Sep. 2005, pp. 66–72.

[15] ——, "Neuro-adaptive dynamic control for trajectory tracking of mobile robots," in *Proc. 3rd International Conference on Informatics in Control, Automation and Robotics (ICINCO'06)*, Setúbal, Portugal, Aug. 2006, pp. 404–411.

[16] ——, "Multilayer perceptron adaptive dynamic control for trajectory tracking of mobile robots," in *Proc. 32nd Annual Conference of the IEEE Industrial Electronics Society (IECON'06)*, Paris, France, Nov. 2006, pp. 3798–3803.

[17] T. Das and I. N. Kar, "Design and implementation of an adaptive fuzzy logic-based controller for wheeled mobile robots," *IEEE Trans. Contr. Syst. Technol.*, vol. 14, no. 3, pp. 501–510, 2006.

[18] F. Lamiraux, J. P. Laumond, C. VanGeem, D. Boutonnet, and G. Raust, "Trailer truck trajectory optimization: the transportation of components for the Airbus A380," *IEEE Robot. Autom. Mag.*, vol. 12, no. 1, pp. 14–21, 2005.

[19] R. Murphy, "Rescue robotics for homeland security," *Communications of the ACM*, vol. 27, no. 3, pp. 66–69, 2004.

[20] P. Debanne, J. V. Herve, and P. Cohen, "Global self-localization of a robot in underground mines," in *Proc. Systems, Man, and Cybernetics - Computational Cybernetics and Simulation*, Orlando, FL, Dec. 1997.

[21] M. Long, A. Gage, R. Murphy, and K. Valavanis, "Application of the distributed field robot architecture to a simulated demining task," in *Proc. IEEE International Conference on Robotics and Automation (ICRA'05)*, Barcelona, Spain, Apr. 2005.

[22] D. Ding and R. A. Cooper, "Electric-powered wheelchairs," *IEEE Control Syst. Mag.*, vol. 25, no. 2, pp. 22–34, 2005.

[23] R. W. Brockett, *Asymptotic Stability and Feedback Stabilisation*, ser. Differential Geometric Control Theory, R. S. Millman and H. J. Sussman, Eds. Boston, MA: Birkhäuser, 1983.

[24] K. J. Åström and B. Wittenmark, *Adaptive Control*, 2nd ed. Reading, MA: Addison-Wesley, 1995.

[25] S. G. Fabri and V. Kadirkamanathan, *Functional Adaptive Control: An Intelligent Systems Approach*. London, UK: Springer-Verlag, 2001.

[26] A. A. Fel'dbaum, "Dual control theory I-II," *Automation and Remote Control*, vol. 21, pp. 874–880, 1033–1039, 1960.

[27] ——, "Dual control theory III-IV," *Automation and Remote Control*, vol. 22, pp. 1–12, 109–121, 1961.

[28] ——, *Optimal Control Systems*. New York, NY: Academic Press, 1965.

[29] N. M. Filatov and H. Unbehauen, "Survey of adaptive dual control methods," in *Proc. IEE Control Theory Applications*, vol. 147, no. 1, Jan. 2000, pp. 118–128.

[30] J. Sternby, "A simple dual control problem with an analytical solution," *IEEE Trans. Autom. Control*, vol. 21, no. 6, pp. 840–844, 1976.

[31] B. Wittenmark, in *5th IFAC Symposium on Adaptive Systems in Control and Signal Processing*, Jan. 1995, pp. 67–72.

[32] A. M. Thompson and W. R. Cluett, "Stochastic iterative dynamic programming: a Monte Carlo approach to dual control," *Automatica*, vol. 41.

[33] N. M. Filatov and H. Unbehauen, *Adaptive Dual Control: Theory and Applications*. London, UK: Springer-Verlag, 2004.

[34] S. G. Fabri and V. Kadirkamanathan, "Dual adaptive control of nonlinear stochastic systems using neural networks," *Automatica*, vol. 34, no. 2, pp. 245–253, 1998.

[35] N. M. Filatov, H. Unbehauen, and U. Keuchel, "Dual pole-placement controller with direct adaptation," *Automatica*, vol. 33, no. 1, pp. 113–117, 1997.

[36] Y. Bar-Shalom and E. Tse, *Concept and Methods in Stochastic Control*, ser. Control and Dynamic Systems, C. T. Leondes, Ed. New York, NY: Academic Press, 1976.

[37] R. Milito, C. S. Padilla, R. A. Padilla, and D. Cadorin, "An innovations approach to dual control," *IEEE Trans. Autom. Control*, vol. 27, no. 1, pp. 133–137, Feb. 1982.

[38] G. A. Dumont and K. J. Åström, "Wood chip refiner control," *IEEE Control Syst. Mag.*, vol. 8, no. 2, pp. 38–43, 1988.

[39] N. M. Filatov, U. Keuchel, and H. Unbehauen, "Dual control for an unstable mechanical plant," *IEEE Control Syst. Mag.*, vol. 16, no. 4, pp. 31–37, 1996.

[40] B. J. Allison, J. E. Ciarniello, P. J.-C. Tessier, and G. A. Dumont, "Dual adaptive control of chip refiner motor load," *Automatica*, vol. 31, no. 8, pp. 1169–1184, 1995.

[41] A. Ismail, G. A. Dumont, and J. Backstrom, "Dual adaptive control of paper coating," *IEEE Trans. Contr. Syst. Technol.*, vol. 11, no. 3, pp. 289–309, May 2003.

[42] M. S. Radenkovic, "Convergence of the generalised dual control algorithm," *Int. J. Control*, vol. 47, no. 5, pp. 1419–1441, 1988.

[43] R. Fierro and F. L. Lewis, "Robust practical point stabilization of a nonholonomic mobile robot using neural networks," *Journal of Intelligent and Robotic Systems*, vol. 20, pp. 295–317, 1997.

[44] K. J. Åström and B. Wittenmark, *Computer Controlled Systems: Theory and Design*, 3rd ed. Upper Saddle River, NJ: Prentice Hall, 1997.

[45] S. Haykin, *Neural Networks: A Comprehensive Foundation*, 2nd ed. London, UK: Prentice Hall, 1999.

[46] R. M. Sanner and J. J. E. Slotine, "Gaussian networks for direct adaptive control," *IEEE Trans. Neural Networks*, vol. 3, no. 6, pp. 837–863, 1992.

[47] R. E. Kalman, "A new approach to linear filtering and prediction problems," *Trans. ASME J. Basic Eng.*, vol. 82, pp. 34–45, 1960.

[48] P. S. Maybeck, *Stochastic Models, Estimation and Control*, ser. Mathematics in Science and Engineering, R. Bellman, Ed. London, UK: Academic Press Inc., 1979, vol. 141-1.

[49] R. Bellman, *Adaptive Control Processes: A Guided Tour*. Princeton, NJ: Princeton University Press, 1961.

[50] A. Field, *Discovering Statistics using SPSS*, 2nd ed. London, UK: Sage Publications Ltd., 2005.

[51] S. J. Julier and J. K. Uhlmann, "A new extention of the Kalman filter to nonlinear systems," in *Proc. of AeroSense: The 11th Int. Symp. on Aerospace/Defence Sensing, Simulation and Controls*, 1997.